

# Effects of Ignition and Wind on the Transition to Flame Spread in a Microgravity Environment

K. B. McGRATTAN\*, T. KASHIWAGI, and H. R. BAUM

*Building and Fire Research Laboratory, National Institute of Standards and Technology, Gaithersburg, Maryland 20899*

S. L. OLSON

*NASA Lewis Research Center, Cleveland, Ohio 44135*

A two-dimensional, time-dependent model is developed describing ignition and the subsequent transition to flame spread over a thermally thin cellulosic sheet heated by external radiation in a microgravity environment. The effects of a slow external wind (0–5 cm/s), and of the flux distribution of the external radiation on the transition are studied mainly in an atmosphere of 30% oxygen concentration. The ignition is initiated along the width of a sample strip, giving rise initially to two flame fronts spreading in opposite directions. The calculated results are compared with data obtained in the 2.2-s drop tower. Both experimental and calculated results show that with a slow, imposed wind, the upstream flame front (opposed mode) is stronger and slightly faster than the quiescent counterpart due to a greater supply of oxygen. However, the downstream flame front (concurrent mode) tends to die during the transition period. For all calculated cases studied in this work using the selected kinetic constants for the global one-step gas phase reaction, the downstream flame front dies out in oxygen concentrations up to 50% and wind velocity up to 5 cm/s. This is caused by the "oxygen shadow" cast by the upstream flame. The ignition delay time depends mainly on the peak flux of external radiation, whereas the transition time to steady state flame spread depends mainly on the broadness of the flux distribution. The broader the radiative flux distribution, the greater the transient flame spread rate due to the preheating of the sample ahead of the flame front by the external radiation and thus the greater the delay to steady state flame spread.

## NOMENCLATURE

$A$	preexponential frequency factor
$c_p$	specific heat, constant pressure
$D$	mass diffusivity
$E$	activation energy
$h$	enthalpy
$k$	thermal conductivity
$\dot{m}$	mass flux
$\dot{q}_R$	absorbed external radiation flux
$R$	universal gas constant
$T$	temperature
$t$	time
$\vec{v}$	velocity vector
$Y$	mass fraction
$\gamma$	reflectivity
$\delta$	half thickness of thin solid sheet
$\epsilon$	emissivity

$\Delta H$	heat of reaction
$\nu$	stoichiometric coefficient
$\rho$	density
$\phi$	velocity potential

## Subscripts

$\infty$	ambient condition
0	initial condition
$s$	solid phase
$p$	solid phase pyrolysis
ox	solid-phase oxidative degradation
char	solid-phase char oxidative degradation
$f$	gaseous fuel
sf	solid fuel
$O_2$	oxygen

## INTRODUCTION

The fire safety strategy in a spacecraft is (1) to detect any fire as early as possible, (2) to keep any fire as small as possible, and (3) to extinguish any fire as quickly as possible [1]. This

\* Corresponding Author: Kevin McGrattan, Building 224, Room A-345, National Institute of Standards and Technology, Gaithersburg MD 20899.

suggests that a material which undergoes a momentary, localized ignition might be tolerable but a material which permits a transition to flame spread would significantly increase the fire hazard in a spacecraft. If the transition does not succeed, flame spread does not occur. Therefore, it is important to understand how the transition from localized ignition to flame spread occurs and what parameters significantly affect the transition.

Although the fundamental processes involved in ignition [2-5] and flame spread [6, 7] have been extensively studied, they were studied separately without combining ignition and flame spread through the transition process. Some of the steady-state flame models start from ignition to reach a steady state, but since the objective of such a calculation is to obtain the steady state flame spread rate, the calculation through the transition process is made without high accuracy to save computational time. Also, the boundary conditions usually used in a steady-state calculation are not appropriate for the transition period. Most often in steady-state models constant velocities or zero velocity gradients are imposed at the boundaries of the calculation. However, because at ignition the expansion field generated by the rapid release of heat impinges on the boundary of the calculation, care must be taken to ensure that the artificial boundary does not interfere with the development of the flames [9]. Attempts to simply pull the boundary far from the reaction zone usually fail because of the fact that the expansion velocity decays inversely to the distance from the heat source, requiring a very large domain to contain the initial expansion.

We have studied the transition from a small localized ignition at the center of a thermally thin paper in a quiescent microgravity environment [9]. The configuration for that study was axisymmetric. However, it has been observed in NASA's drop tower experiment that a slow external flow can significantly enhance the flame spread rate [10]. Thus, a slow external flow comparable to a ventilation flow in a spacecraft has been added to our previous model and both two- and three-dimensional time-dependent numerical codes have been de-

veloped. The effects of the radiative source distribution, atmospheric oxygen concentration, and external wind on the transition from ignition to flame spread over a thin cellulosic sheet are studied in this work.

In previous flame spread studies in microgravity, two-dimensional flame spread was initiated by ignition at one end of a sample with or against a slow external flow [10]. In this experimental configuration, there is only one flame front. However, if ignition is initiated away from either end of the sample, there could be two different flame fronts spreading in opposite directions from the ignition area simultaneously; one flowing downstream in a concurrent mode, and the other upstream in an opposed mode. This configuration might be more realistic than the one flame front case because there might be some interaction between the two fronts. In fact, we will demonstrate that under certain conditions a flame originating at either end of a sample strip will propagate, with or against the external flow; whereas when the flame originates from the center of the strip, the front propagating against the wind will survive the transition to flame spread whereas the front propagating with the wind will not.

Both numerical and physical experiments have been conducted for the two-dimensional configuration and the results are discussed below. We will restrict discussion in this paper to the two-dimensional case, and present the three-dimensional results in a future paper.

## MODEL DESCRIPTION

A complete description of the mathematical model has been given in Ref. 9. A brief outline of the relevant methodology is given here. First, the gas phase is governed by the conservation equations of mass, energy, and species (fuel gases and oxygen) under low Mach number combustion and heat transfer conditions, which can be written

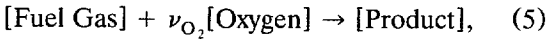
$$\frac{D\rho}{Dt} + \rho \nabla \cdot \vec{v} = 0, \quad (1)$$

$$\rho \frac{Dh}{Dt} - \nabla \cdot (k \nabla T) = \Delta H_f \dot{m}_f + \dot{q}_R \quad (2)$$

$$\rho \frac{DY_{O_2}}{Dt} - \nabla \cdot (\rho D \nabla Y_{O_2}) = -\nu_{O_2} \dot{m}_f \quad (3)$$

$$\rho \frac{DY_f}{Dt} - \nabla \cdot (\rho D \nabla Y_f) = -\dot{m}_f \quad (4)$$

where  $h = \int_0^T c_p(T) dT$ . The gas-phase oxidation reaction is represented by a global one-step reaction



characterized by an Arrhenius rate term

$$\dot{m}_f = A \rho^2 Y_{O_2} Y_f \exp\left(-\frac{E}{RT}\right). \quad (6)$$

These conservation equations are supplemented by an equation of state, taken in a form appropriate for low Mach number flows

$$\rho h = \rho_x h_x. \quad (7)$$

This assumption leads to a Poisson equation for the velocity potential  $\phi$

$$\nabla^2 \phi = \frac{\Delta H_f \dot{m}_f + \dot{q}_R + \nabla \cdot (k \nabla T)}{\rho_x h_x}, \quad (8)$$

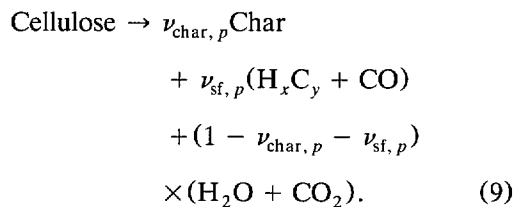
which relates the potential field to the temperature distributions in the gas phase. Implied in this statement is the assumption that the solenoidal velocity field is not of interest; otherwise there is no alternative to solving the Navier–Stokes equations. Thus, the velocity  $\vec{v}$  is solely the gradient of the potential  $\phi$ . Because of this, it is easy to superimpose an external wind onto the flow induced by the heated surface and gas-phase reaction. A detailed analysis of the potential flow approximation can be found in Ref. 12.

The absorption of the external radiation by evolved degradation products in the gas [2, 13] is not included in the model because a tungsten lamp, which emits the majority of its energy in the near infrared, will be used to reduce the absorption as much as possible during the ignition period in the planned experiment. After ignition, the external radiation is reduced as the sample paper is consumed; thus

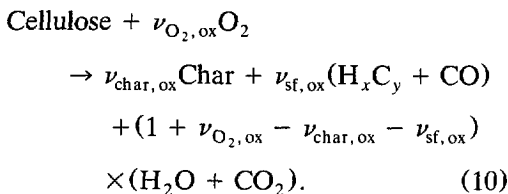
the absorption of the external radiation by the combustion products such as soot does not significantly affect the transition process. Under these circumstances, the term  $\dot{q}_R$  can be neglected. It has been reported that the radiation from the flame to the sample surface ahead of the flame is important for low opposed flow based on model results or measured surface temperatures in microgravity [7]. However, the directly measured radiant flux from the edge of a 30-cm methanol pool flame shows very small radiant flux, about 2 kW/m<sup>2</sup> in normal gravity [8]. This blue flame radiates mainly from the water and CO<sub>2</sub> bands, which were used in the calculations of the microgravity flame, and the size of the methanol flame is about two orders of magnitude larger than the microgravity flame. Therefore, it is not certain whether the radiative feedback in the opposed flow configuration is important or not. However, since the flame becomes bright yellow, indicating radiation from soot particles in a concurrent flow configuration, the radiation from such a flame could be important. At present, radiative feedback is not included in the model. If its importance is clearly demonstrated by experiments rather than by model results alone which are based on overly simplified one-step gas phase kinetics, the radiative feedback will be included in the model.

The boundary conditions for the gas-phase equations are provided by the solid fuel reactions. It is assumed that the cellulosic sheet is thermally thin and also of uniform composition through its depth. The pyrolysis of the cellulosic sheet is described by two global thermal degradation reactions and a char oxidation reaction. The detailed derivation of these reactions and their kinetic constants are described in Ref. 15. A brief description of the reaction model is given here.

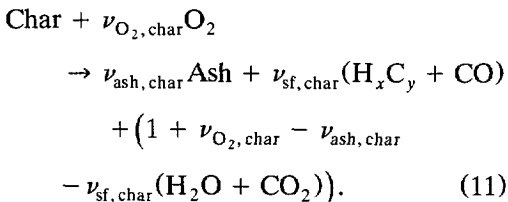
1. *Endothermic global pyrolysis reaction:*



2. *Exothermic global thermal oxidative degradation reaction:*



3. *Exothermic global char oxidation reaction:*



The combustible gases consist of hydrocarbons ( $\text{H}_x \text{C}_y$ ) and CO and the noncombustible gases consist of  $\text{CO}_2$  and  $\text{H}_2\text{O}$ . It is assumed that the combustible gases formed from each reaction above are the same. Although these reactions are grossly approximated compared with the actual, extremely complex degradation reactions, their accuracy is at least comparable to that of the global one-step gas-phase oxidation reaction for the combustible gases, which is used as the sole gas-phase reaction in this study. The reaction rates for the three solid-phase reactions are Arrhenius expressions and are given in Ref. 15. Radiative loss from the sample surface is included in the model, and the emissivity of the fuel is assumed to be one.

The geometrical configuration for the two-dimensional simulations is intended to mimic the experiments conducted in the NASA's 2.2-s drop tower, in which a sample strip is heated along its width by a radiative source. This study differs from previous studies in that the strip is ignited halfway along its length, giving rise to two oppositely directed flames. This will be of importance in the discussion of the transition to flame spread. The radiative heat flux distribution is assumed to be Gaussian with a prescribed peak and half-width<sup>1</sup> which are typically on the order of 20 W/cm<sup>2</sup> and 0.25 cm,

respectively. This sharp flux profile is intended to mimic the experiments in which a pilot wire is used to heat the sample. Variations of this initial flux profile will be considered below.

The reflectivity of the sample is assumed to be 0 and the emissivity is assumed to be 1. The thickness of the cellulosic material used in the present study is 0.0076 cm. Its initial density is 0.263 g/cm<sup>3</sup> and specific heat 1.26 J/(g · K). It is assumed that this value of specific heat applies to the char and ash, as well. At time  $t = 0$ , the entire system is at ambient temperature 300 K, the gas phase fuel mass fraction  $Y_f$  is zero, and the oxygen mass fraction and the velocity of the external wind are prescribed.

The specific heat of the gas  $c_p$ , the density  $\rho$ , thermal conductivity  $k$ , and diffusivity  $D$  are considered functions of the temperature  $T$ , and they are fitted by polynomial expressions. We assume that the gas has the same properties as air. At ambient temperature,  $c_p = 1.01$  J/(g · K),  $\rho = 1.19 \times 10^{-3}$  g/cm<sup>3</sup>,  $k = 2.63 \times 10^{-4}$  W/(cm · K), and  $D = 0.17$  cm<sup>2</sup>/s. The kinetic constants for the global gas phase oxidation reaction are arbitrarily selected to be:  $A = 5.0 \times 10^9$  cm<sup>3</sup>/(g · s),  $E = 6.7 \times 10^4$  J/mol,  $\Delta H_f = 3.5 \times 10^4$  J/g, and  $\nu_{\text{O}_2} = 3.57$ . These values are slightly different than those used in Ref. 9 in that the gas phase reaction rate has been slightly increased. It has been observed that the ignition and transition to flame spread is very sensitive to the choice of the gas phase reaction constants. The present choice is guided by a desire to roughly match flame spread rates with the experiments of Olson [10] in 30% oxygen. However, the objective of the study is not necessarily to duplicate quantitative experimental results exactly by manipulating the model parameters, but rather to deduce trends of the transient phenomena. In fact, given the one-step Arrhenius reaction rate for the gas-phase oxidation, Eq. 6, small changes in flame temperature are amplified according to the relation

$$\frac{\delta \dot{m}_f}{\dot{m}_f} \approx \left( \frac{E}{RT} - 2 \right) \frac{\delta T}{T} \quad (12)$$

where  $\delta T$  and  $\delta \dot{m}_f$  are small changes to these quantities. The factor on the right is about 2.5 for temperatures near 1800 K. Furthermore,

<sup>1</sup>The half-width is taken as the distance from the center point at which the flux drops to  $e^{-1}$  its original strength.

the degradation process of cellulose is extremely complex and the evolved degradation product composition changes with temperature [14]. Water is the major degradation product initially, after which many small to large organic molecules are generated. Since a cellulosic material generates char having a carbon-rich structure, the elemental composition of its degradation products changes with its temperature and mass fraction. On the other hand, the elemental composition is nearly constant for non-char-forming materials such as polyethylene or polymethacrylate. Thus, any attempt to "fine tune" the global, one-step gas-phase reaction kinetic constants for the transient heating of a cellulosic material is a rather pointless exercise. Moreover, an exact quantitative prediction of the transition from ignition to flame spread over a cellulosic material using a global one-step reaction scheme based on the original elemental composition of the cellulose is impossible. In the examples to follow, we seek to show qualitative or at best semiquantitative agreement between experiment and numerical simulation.

The numerical algorithm used to solve the above solid- and gas-phase reaction and evolution equations is described in Ref. 9. Briefly, the three solid-phase degradation reactions are written as a system of conservation equations for mass, cellulose, char, and energy, and solved using a stiff ordinary differential equation solver. The equations for the gas-phase temperature and species (2-4) are written in finite difference form and solved with a simple time splitting scheme in which it is assumed that the oxidative reaction occurs over a small part of the overall time step, and the convective and diffusive terms are differenced and updated with an ADI (Alternating Direction Implicit) scheme. Equation 8 is solved using an efficient Poisson solver. Boundary conditions for the velocity potential at the open boundaries are computed directly from the Greens function formulation of the solution. Details may be found in Ref. 9.

To resolve steep gradients in the direction normal to the sample surface, the domain is non-uniformly gridded in the normal direction. Typically, cells near the surface are about 0.5-1.0 mm in the direction parallel to the

surface and about 0.1-0.3 mm in the normal direction. Calculations were done to ensure that the results did not depend on grid cell size or time step. Because three-dimensional calculations are presently being performed on grids of comparable spacing, grid sensitivity studies in two dimensions are extremely valuable because they indicate whether or not adequate resolution is being maintained. Two-dimensional calculations take only a few hours to perform on an IBM RISC/6000 workstation, while three-dimensional calculations of comparable resolution can take tens of hours.

## EXPERIMENTAL DESCRIPTION

A series of experiments was conducted in the NASA Lewis Research Center's 2.2-s Drop Tower Combustion Tunnel apparatus (previously described in Ref. 16) to study the effects of low-velocity flow on flame spread over thermally thin solids, in this case tissue paper. To obtain both upstream and downstream flame front propagation simultaneously in a single test, the fuel was centrally ignited by a straight nichrome wire run across the full width, 7.5 cm from each end. In this planar configuration the downstream (concurrent) flame front could be influenced by the upstream (opposed flow) flame. Flows of 0, 2, or 5 cm/s were imposed parallel to the length of the sample; molar concentrations of oxygen were 21 or 30% in N<sub>2</sub>. The fuel was a 5-cm-wide by 15-cm-long cellulose sheet (Kimwipe) with an area density of  $1.998 \times 10^{-3}$  g/cm<sup>2</sup> [10].

## RESULTS AND DISCUSSION

### External Wind Effects

In the two-dimensional configuration the effects of a slow external wind on the transition and the flame spread are examined over a strip which is ignited along its width. As a first example, consider the radiant ignition of a strip in an atmosphere of 30% oxygen. Figure 1 displays the evolution of the flame front during the transition period for the case of an imposed wind of 2 cm/s blowing from left to right along the length of the strip (right sequence) and for the case of a quiescent environment (left sequence). At 0.5 s after the

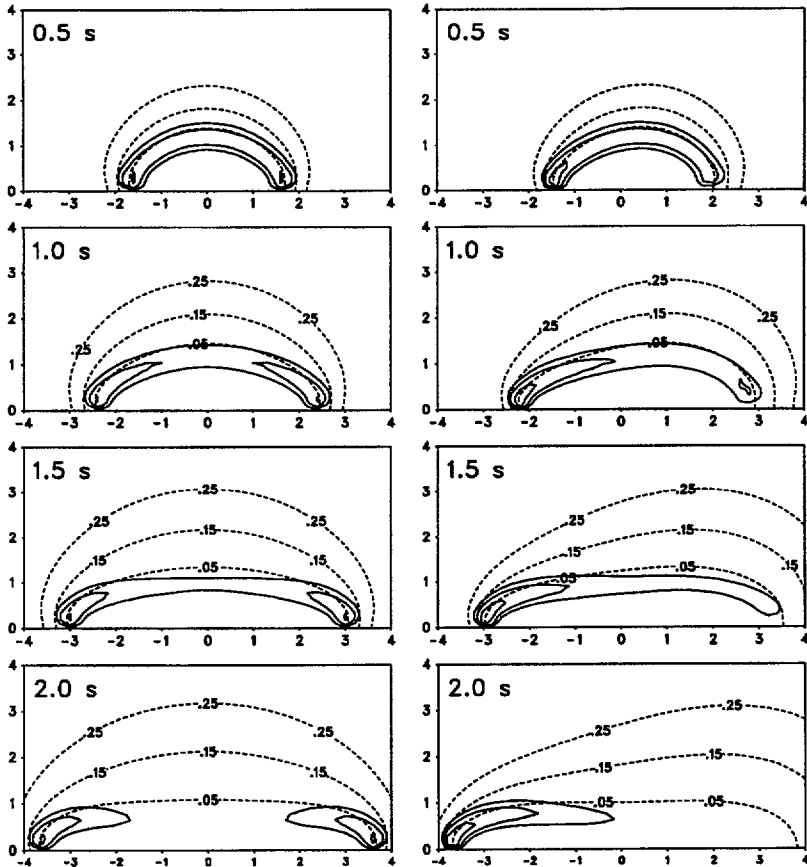


Fig. 1. A comparison of the transition period with and without an imposed wind. The sequence on the left shows the generation of two flames in a quiescent environment, while the sequence on the right is subjected to a 2 cm/s wind blowing from left to right. The dashed lines indicate oxygen mass fraction, the solid lines indicate gas-phase reaction rate for  $\dot{m}_f = 10^{-4.5}, 10^{-4}$  and  $10^{-3.5}$  g/(cm<sup>3</sup> · s). The outer reaction contour roughly corresponds to the visible flame. The ambient oxygen concentration is 30%.

imposition of the external radiation, both flames take on an arch-like shape, and two flame fronts emerge in each case. The quiescent flame is symmetric, the windblown flame is slightly deflected downstream. At 1.0 s, the gas phase reaction rate in the center part of the quiescent flame decreases. However, for the windblown flame, the downstream flame front weakens as evidenced by the decreasing gas phase reaction rate. At the same time, the upstream flame front strengthens compared to the quiescent counterpart. As time passes, these trends continue. The downstream flame front eventually disappears (i.e., the gas-phase reaction rate drops below  $10^{-4.5}$  g/cm<sup>3</sup> s) while

the upstream flame propagates into the wind at a speed of 1.5 cm/s, faster than the quiescent counterpart (1.2 cm/s). The propagation history of the two flame fronts for both cases is shown in Fig. 2.

Snapshots of the drop tower experiment for the windblown case are shown in Fig. 3. Although ignition is not achieved symmetrically with respect to a thin tissue paper (the left side ignited earlier than the right side), nearly symmetric flames appear about 1.25 s later. At about 1 s, the left side flame shows clearly two blue color flame fronts; one toward the upstream and the other toward the downstream. This left side flame is similar to the calculated

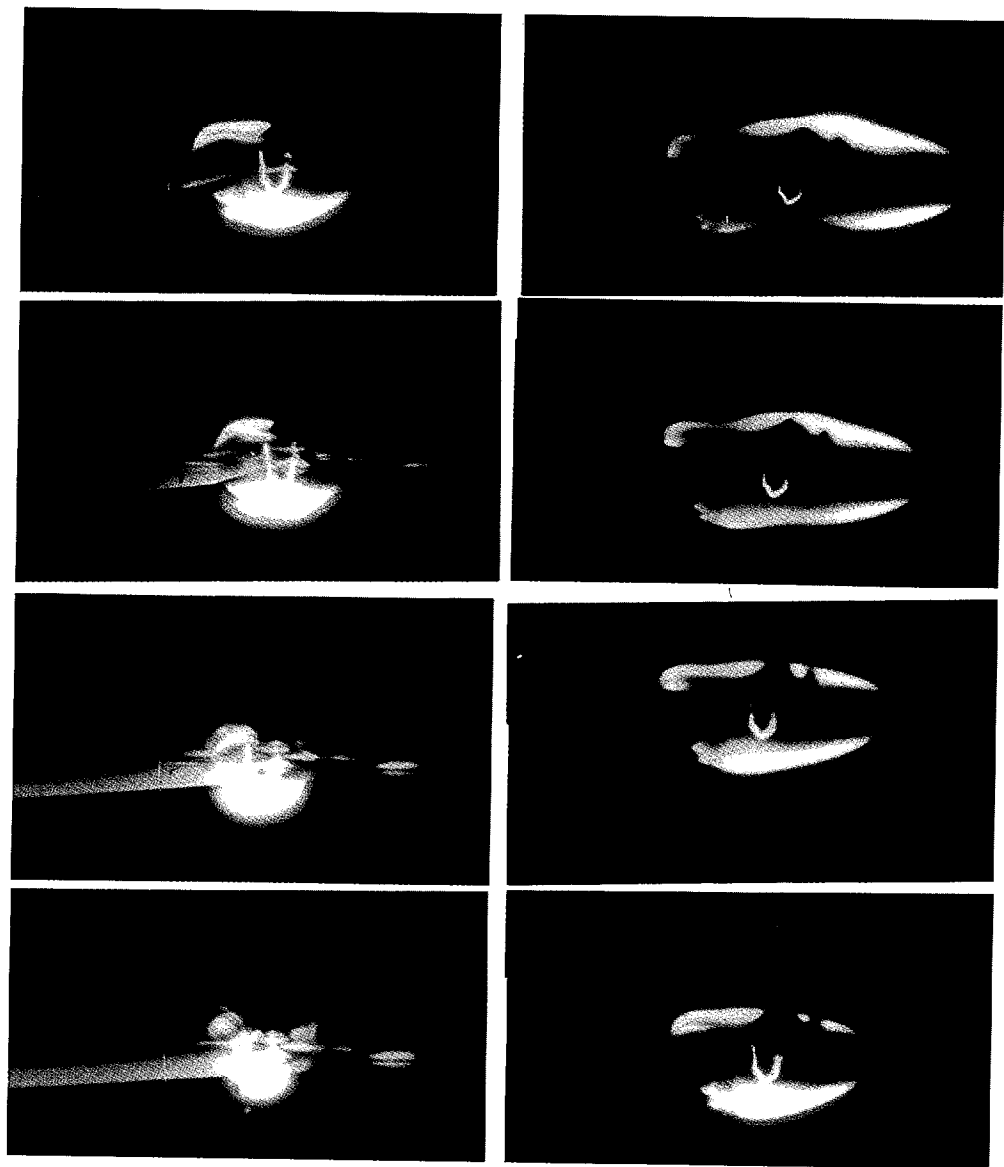


Fig. 3. Snapshots of a 2.2-s drop tower experiment. Shown is the ignition of a strip of tissue paper with an imposed wind of 2 cm/s blowing from bottom to top in an atmosphere of 30% oxygen. The pictures were taken 0.25 s apart, from ignition to impact.



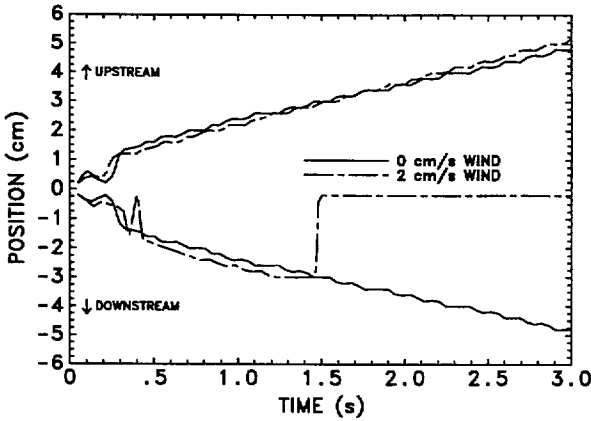


Fig. 2. A comparison of the flame propagation profiles for simulations with external winds of 0 and 2 cm/s in 30% oxygen. The position of each flame front is taken as the horizontal distance from the ignition point to the point of maximum gas phase reaction rate  $\dot{m}_f$ . The flame spread rate for the quiescent flame is about 1.2 cm/s whereas that for the windblown case is about 1.5 cm/s.

flame shape at 0.5 s for the 2 cm/s wind case in Fig. 1.<sup>2</sup> In Fig. 3, the flame gradually spreads along the sample and at about 1.5 s the downstream blue flame front becomes faint similar to the windblown calculated results at 1 s. At about 2 s in the experiment, the downstream blue flame front has almost disappeared and only a windblown sooty flame is visible. During the short available test time of this particular drop tower experiment, it is not clear if the fading downstream flame front would continue to propagate. Plans are underway to conduct longer experiments in both longer drop towers and aboard the Space Shuttle to determine ultimate behavior of the two flame fronts. A time history of the flame fronts for the experiment is plotted in Fig. 4. The downstream flame spread rate is defined here as being the movement of the visible downstream flame tip. The upstream windblown flame propagates at about 2.1 cm/s whereas the quiescent flame propagates at about 1.9 cm/s. The downstream windblown flame propagates more slowly than the quiescent flame, and it is still in the transition period at the end of the test.

It is important to understand why the upstream flame front appears to be stronger and slightly faster than the quiescent flame front, and why the downstream flame front appears to be weaker than the quiescent flame front and eventually is extinguished. The upstream

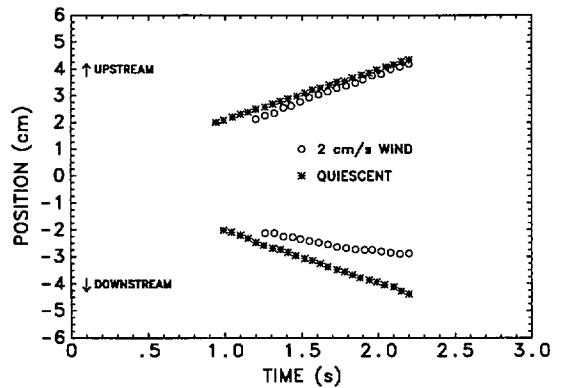


Fig. 4. Experimental flame propagation profile showing the positions of the upstream and downstream flame fronts in 30% oxygen for wind speeds of 0- and 2-cm/s wind. The upstream flame in the 2-cm/s wind is spreading at a rate of about 2.1 cm/s whereas the quiescent flame is spreading at about 1.9 cm/s.

flame fronts for both the windblown and quiescent cases are shown in Fig. 5. Included in the figure are contours of the oxygen mass fraction  $Y_{O_2}$ . The distribution of the oxygen contours shows that the oxygen gradient in front of the windblown flame is greater than that for the quiescent flame. The windblown flame is about twice as strong as the quiescent flame, as measured by the peak gas phase reaction rate  $\dot{m}_f$ . Also, its maximum temperature is about 1780 K whereas the quiescent flame is about 1570 K. Furthermore, the windblown flame is closer to the sample surface than the quiescent flame, providing a greater conductive heat feedback from the flame. The calculated peak feedback rate for the windblown flame is about 3.5 W/cm<sup>2</sup>, whereas that for the quiescent flame

<sup>2</sup>The ignition times and external heat flux differ in the experiment and simulation. The energy input from the wire was not well-defined due to the transient change in contact between the wire and the sample.

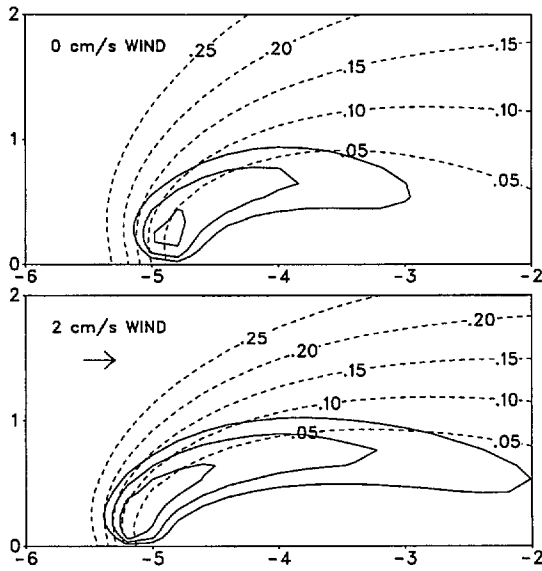


Fig. 5. Closeup of the upstream flame fronts for simulations with and without a 2-cm/s imposed wind. Included are the reaction rate contours as above (solid lines), along with the oxygen mass fraction (dashed lines). The ambient oxygen concentration is 30%.

is about  $2.5 \text{ W/cm}^2$ . It has been observed in the experiments that the external wind tends to increase the overall length of the flame and reduce the flame standoff distance [16, 17]. Both these effects are observed in the numerical simulations as well.

The effect of a slow external wind on the downstream flame front is more complex than that for the upstream flame due to possible interaction between the two flame fronts. Therefore, numerical simulations were performed in which the sample strip was heated at one end and an external wind prescribed in the same direction as the flame spread. This allows us at first to understand the effect of the external wind without any interference from an upstream flame. Figure 6 displays the computed oxygen mass fraction contours, along with the gas phase reaction zones, of three cases with winds of 0, 1 and 5 cm/s. The case of no wind represents an opposed flow, because in flame fixed coordinates the flame encounters a flow equal to its spread rate. The case of a 5-cm/s wind represents a concurrent flow, because the wind speed is faster than the spread rate. The 1 cm/s case is neither concurrent nor opposed because the wind speed is

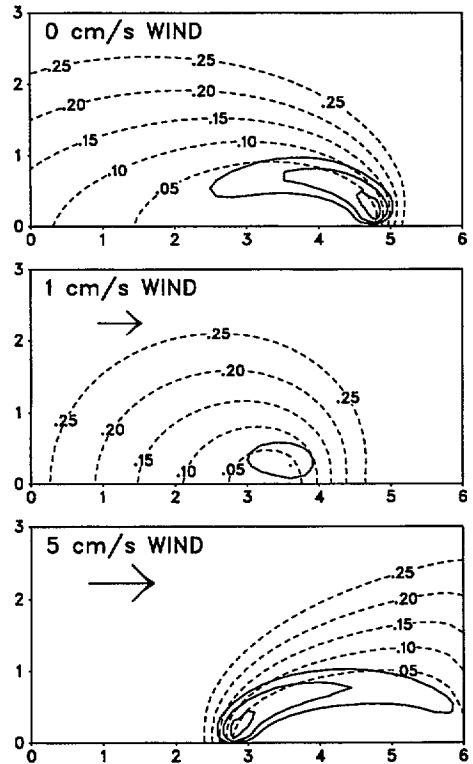


Fig. 6. Computed oxygen mass fraction (dashed lines) and reaction rate (solid lines) for three single flame front simulations. The ambient oxygen concentration is 30%, and the flame shown occurs 4 s after the start of the simulation.

about the same speed as the flame spread rate (at least before the flame dies out). The transition from ignition to flame spread succeeds for the 0- and 5-cm/s cases, but does not for the 1-cm/s case. A time history of the 1 cm/s case is shown in Fig. 7. At 1 s, a relatively strong flame front is observed but the flame becomes progressively weaker with time. It is clear from the oxygen contours why the 1 cm/s case extinguishes—the oxygen is unable to penetrate the reaction zone in sufficient amount to maintain combustion. The flame exposed to a 5-cm/s external wind is strengthened by increased convective transport of oxygen due to the wind, and by the preheating of the sample, again due to the wind. The present model contains no mechanism for gas-phase radiative heating of the sample; thus it remains unclear how important this effect would be in preheating the sample compared to the convective/diffusive transport of heat.

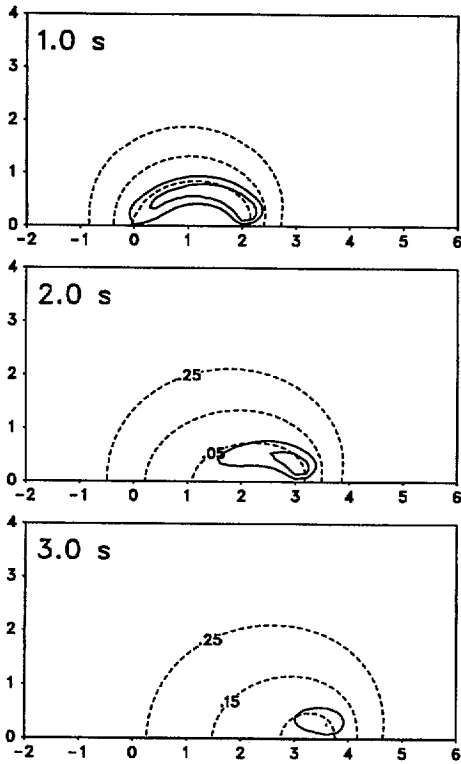


Fig. 7. Time history of a single flame propagating from left to right with a wind of 1 cm/s moving in the same direction. Shown are contours of gas-phase reaction rate (solid lines) and oxygen mass fraction (dashed lines). The reaction rate contours correspond to  $\dot{m}_f = 10^{-4.5}$ ,  $10^{-4}$ , and  $10^{-3.5}$  g/(cm<sup>3</sup> · s). The ambient oxygen concentration is 30%.

About a dozen of these one-flame simulations were performed for winds directed both with and against the direction of flame spread. The spread rate of each flame front (assuming it survives the transition period) can be defined in terms of a characteristic relative velocity [16], which is the difference between the flame front velocity and the wind velocity. For example, a flame advancing into the wind has a positive characteristic relative velocity which is equal to the wind speed plus the flame speed. This flame falls into the opposed flow regime. On the other hand, a flame advancing in the same direction as the wind can be either opposed or concurrent. If the wind speed is greater than the flame speed, the flow is concurrent, and the c.r.v. is negative. If the wind speed is less than the flame speed, the flow is opposed, and the c.r.v. is positive. The calculated relationship between the characteristic relative velocity and flame spread rate is shown in Fig. 8. There is a range of c.r.v. in which steady-state flame spread does not occur (shaded area). The flame shown in Fig. 7 is a good example of this regime. The width of this band depends on the selected kinetic constants for the gas-phase reaction. For example, a lower heat of combustion or higher stoichiometric ratio would make the unsuccessful transition region wider. For values of c.r.v. greater

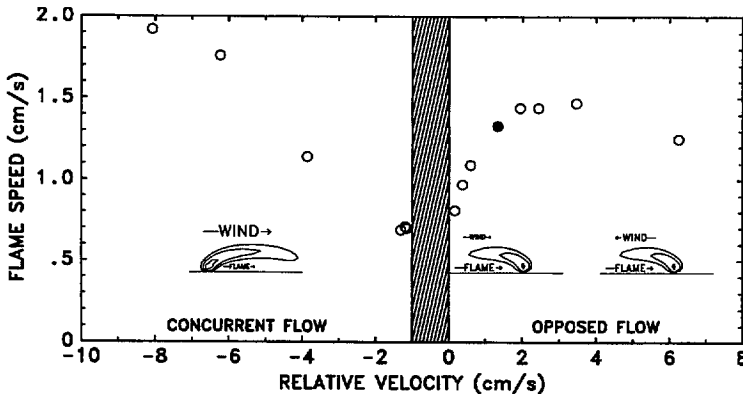


Fig. 8. Comparison of flame speed for a single flame ignited at the end of the sample strip versus the characteristic relative wind velocity, that is, the vector difference of flame and wind velocity. The no-wind case is blackened. The shaded zone indicates that steady-state flame spread is not achieved. The two types of opposed flow shown by the diagrams to the right of the shaded region represent relative velocities to the left and right of the no wind point.

than about 0 cm/s (i.e., opposed flows), there is an increase in flame spread rate with greater opposed flow velocity until a maximum is reached beyond which the spread rate decreases. For the concurrent flow regime to the left of the band of unsuccessful c.r.v. values, the flame spread rate increases steadily with larger concurrent wind speeds.

The calculated trends shown in Fig. 8 agree well with previous experimental results. Olson's experiments in 30% oxygen [16] show an increase in flame spread rate with external wind speed in the low-speed opposed flow regime, topping off for wind speeds of about 3–4 cm/s. Olson also reports an experiment in 30% oxygen in which a wind is directed in the same direction as the flame spread, and the wind speed is slightly slower than the flame speed (char. relative velocity is 0.1 cm/s). She notes that the flame is very sooty, and propagates more slowly than the opposed flow counterparts. The data of Grayson, et al. [20] indicate that concurrent spread rates in air and at 30% oxygen are slightly lower than the opposed flow counterparts for relative velocities less than 5 cm/s. It is interesting to point out that the calculated flame spread rate in the opposed flow regime has a peak value without including flame radiation. In Ref. 18, it is reported that flame radiation is needed to obtain such a trend in flame spread rate for a thermally thin sample. It appears that her calculation did not include wind velocities below 4.5 cm/s and did not observe this trend. Also, the value of absorption coefficient of  $10 \text{ m}^{-1}$  for the flame used in her study appears to be exceedingly large. More appropriate values are in the range  $0.1\text{--}1.0 \text{ m}^{-1}$  [19].

The above results in 30% oxygen show that when the sample strip is ignited at one end, the transition from ignition to flame spread for concurrent flames occurs except in a narrow range where the wind and flame velocities are nearly the same. However, when the strip is ignited in the middle and two flame fronts emerge, the downstream flame front always tends to die out for atmospheres of 30% oxygen and imposed winds less than 5 cm/s. These results indicate the significant influence of an "oxygen shadow" cast by the upstream flame front on the downstream. Figure 9 shows the

calculated contours of gas phase reaction rate and oxygen concentration for the case of flames ignited at the end and in the middle of the sample strip. The oxygen concentration is 30% and the wind speed is 2 cm/s. Initially, the mid-strip flame is larger since there is more fuel available. Even so, two flame fronts appear in both configurations, but in both cases, the downstream flame fronts disappear. Therefore, the "oxygen shadow" effect occurs in both cases. It is interesting that in both cases the upstream flame fronts are subjected to steeper oxygen gradients and survive the transition, whereas the downstream fronts do not. In fact, the mid-strip upstream flame (left) is stronger than the concurrent flame which is generated at the end of the strip (right), as evidenced by the steeper oxygen gradient.

Since the supply of oxygen to the downstream flame front is critical, a higher ambient oxygen concentration might increase the likelihood of its survival. The behavior of the two flame fronts during the transition period in 50% oxygen with 2 cm/s wind is shown in Fig. 10. (Note that the computational domain is much larger than the area shown in this figure.) Both upstream and downstream flame fronts travel rapidly in opposite directions. The upstream flame is much stronger than the downstream flame (the peak gas phase reaction rate for the upstream flame is at least one order of magnitude larger than that of the downstream flame) but flame spread rate is not significantly different from each other. At 3 s, the downstream flame becomes very weak and further continuation of the calculation shows that this flame dies out. Although the exact limit of the survival of the downstream flame depends on the definition of flame and also on the selected kinetic constants for the gas-phase reaction, it is clear that the downstream flame tends to die out due to the influence of the upstream flame (the dilution by the combustion products and consumption of oxygen) when the strip is ignited in the middle.

### Effect of Radiative Source on Ignition

Because a great emphasis of this work is on transient effects, it is important to understand how the mode of ignition influences the devel-

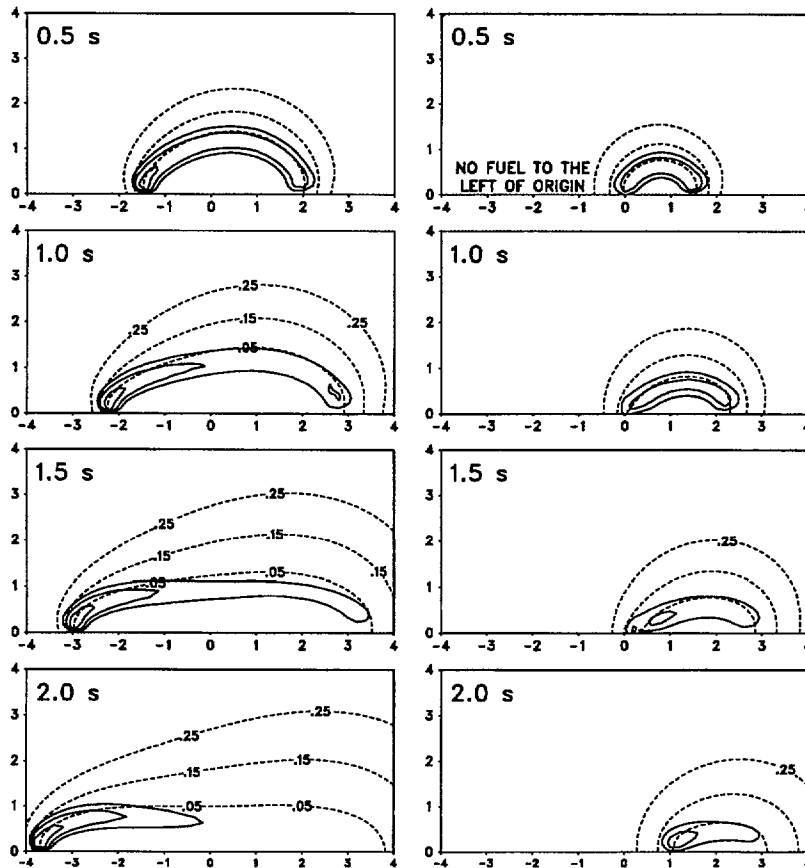


Fig. 9. The sequence on the left shows the transition sequence for a mid-strip ignition with an imposed wind of 2 cm/s. The sequence on the right shows the same case, except that there is no fuel present to the left of the origin, i.e., the origin now represents the end of the strip instead of the middle. The dashed lines indicate oxygen mass fraction, the solid lines indicate the gas phase reaction rate as above. The ambient oxygen concentration is 30%.

opment of the flame in the transition period. Unfortunately, it is very difficult to study this period experimentally, especially since most flame spread experiments make use of a pilot wire to ignite the sample, whereas in a numerical simulation it is more convenient to simply prescribe a distributed heat flux at the sample surface. To simulate the rapid ignition by a pilot wire, a sharp radiative flux profile has been used in the simulations discussed above. This mode of ignition simulates piloted ignition reasonably well because the delay time is small and the flames quickly achieve steady-state spread. However, it is possible to ignite the sample with a less sharp profile and study the effect on the transition period.

First, five unpiloted radiative ignition runs were conducted in which the width of the Gaussian radiative source was altered, but the integrated heat flux was held constant. The half-widths of the profiles varied from 0.25 cm to 5 cm. The results are summarized in Fig. 11. Ignition is achieved most rapidly by a sharp radiative flux distribution with a peak flux of 20 W/cm<sup>2</sup>. However, for a wider profile with lower peak flux, the ignition delay time is longer, the flame spread rate during the transition period is increased, and it takes a longer time to attain steady-state flame spread.

To show this, the distributions of gas phase temperature and reaction rate near the irradiated area are plotted shortly after ignition and

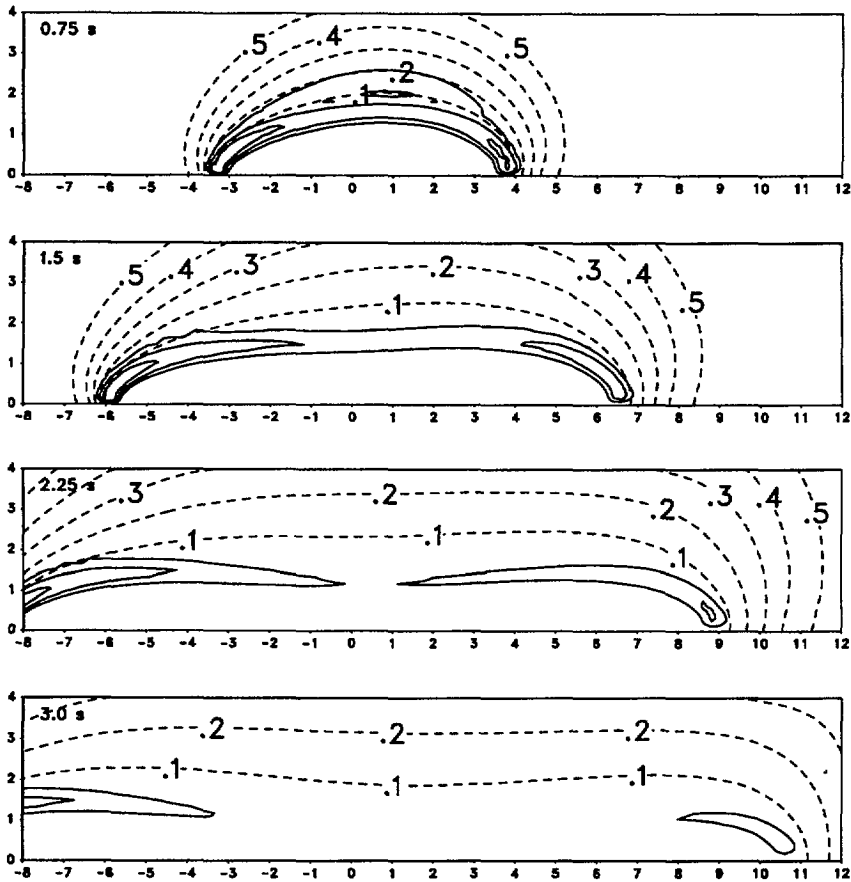


Fig. 10. Transition sequence for a two-flame case with an imposed wind of 2 cm/s and an ambient oxygen concentration of 50%. The dashed lines indicate oxygen mass fraction, the solid lines indicate the gas phase reaction rate as above.

shown in Fig. 12. The figures show that an increase in gas-phase temperature is limited to slightly beyond the flame region for the sharp profile. On the other hand, an increase in gas-phase temperature for the wide profile ex-

tends well beyond the flame region, particularly along the sample surface ahead of the flame front. The surface temperature of the preheated sample is not high enough to initiate thermal degradation of the sample, and the

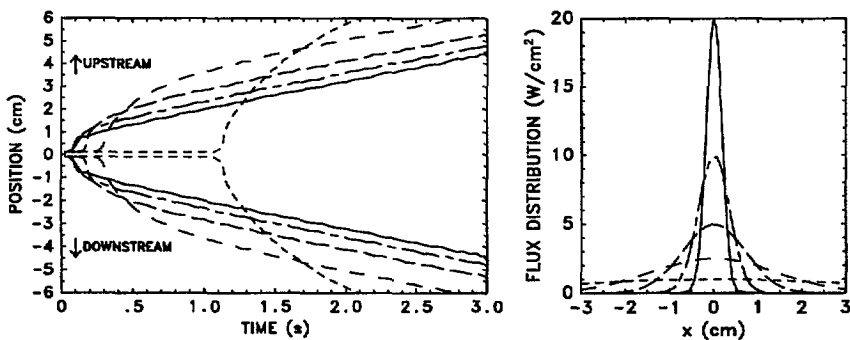


Fig. 11. Flame spread profiles for various radiative source distributions, all of which have the same integrated heat flux. The ambient oxygen concentration is 30%; there is no external wind.

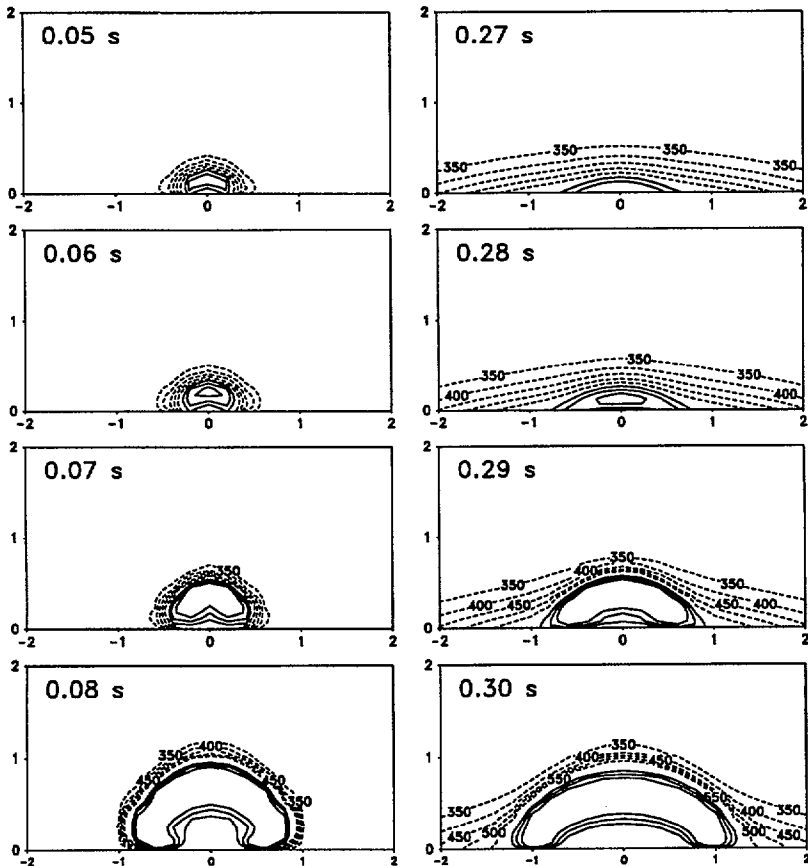


Fig. 12. The reaction zones and temperature fields for two simulations of different radiant flux distributions. The left-hand flame is generated by an initial radiative flux with a peak of 20 W/cm<sup>2</sup> and half-width of 0.25 cm. The flux for the right-hand flame has a peak of 2.5 W/cm<sup>2</sup> and half-width of 2.0 cm. The flux distribution in both cases is centered about the origin  $x = 0$ , and the flame front is symmetric about this point for the no-wind case. The solid contours refer to the logarithm (base 10) of the reaction rate  $\dot{m}_f$  (shown here -4.5, -4.0, -3.5) and the dashed contours to temperature in degrees Kelvin.

ignition is delayed. When ignition does take place, a large area of the sample is preheated. It has been pointed out by Bhattacharjee et al. [7] that for low-speed flame spread heat loss in front of the flame has a significant impact on the steady-state spread rate. They note that more preheating of the sample surface in front of the flame causes an increase in flame speed and a widening of the overall flame. This is consistent with the observations of the calculated transient flames discussed above. Thus, the high flame spread rate during the transition period for the sample ignited with the wide profile is due to preheating of the sample surface. Eventually, however, the flame front passes over the preheated area and slows down

to a flame speed equal to that of a flame ignited by a sharp flux profile.

As a further check on the effect of the source strength and distribution, several runs were made holding the peak flux constant and varying the half-width; and several runs were made holding the half-width constant and varying the peak flux. For the case of fixed peak flux, the ignition delay time is about the same for each run, but the broader source serves to preheat a greater area of the sample and the flame front spreads faster during the transition period just after ignition. For the case of fixed half-width, the ignition time is determined primarily by the peak flux, but the peak flux does not significantly affect the transition process

since there is no difference in the preheat zone. When subjected to an imposed wind of 2 cm/s, the downstream flame front initiated by ignition with a sharp flux profile dies out in 30% oxygen as shown above. With the wider flux profile, the downstream flame front travels farther and survives longer, but it eventually dies when it reaches the end of the preheat zone. The preheating of the sample is not enough to overcome the effect of the "oxygen shadow" cast by the upstream flame.

## CONCLUSION

The numerical model outlined in this paper has been useful in making qualitative predictions of transient behavior of ignition and transition to flame spread. Hopefully, a better understanding of the gas phase reaction mechanism will enable quantitative predictions, as well.

When localized ignition is initiated in the middle of the sample strip in the presence of an imposed wind, the upstream flame front (opposed mode) is stronger and faster than the quiescent counterpart due to a greater supply of oxygen to the flame front. However, the downstream flame front (concurrent mode) tends to die. For all cases studied in this work with the given gas-phase kinetics, the downstream flame front dies out during the transition period in oxygen concentrations up to 50% and wind velocities up to 5 cm/s. The "oxygen shadow" cast by the upstream flame front is largely responsible for this. The same effect also applies to a flame originating at the upstream end of a sample strip. Whether the flame propagates in opposed or concurrent mode depends on which flame front becomes anchored during the transition period. For a narrow range of wind velocities, neither front will become anchored, in which case neither front survives the transition. In this case, the wind speed and flame spread rate are nearly the same, and the oxygen supply to the flame is greatly reduced, as evidenced by the small oxygen gradients normal to the flame front. The range of relative velocity in which a flame originating at the end of the strip does not survive the transition depends on the selected kinetic constants of the global one-step gas

phase reaction and oxygen concentration. A higher stoichiometric coefficient or lower oxygen concentration tends to widen the range.

The transition from ignition to flame spread when ignition is initiated by a sharp, narrow flux distribution is relatively short, comparable to a piloted ignition, whereas the ignition is delayed and the transition period is longer when the radiative profile is wider and the peak flux lower. The transient flame spread rate is greater during this transition period due to the preheating of the sample ahead of the flame front. Therefore, the flame front in the latter case extends farther than that in the former case at comparable times from ignition. The ignition delay time depends mainly on the peak flux, whereas the transition time to steady state flame spread depends mainly on the broadness of the flux distribution. The broader the radiative flux distribution, the greater the delay to steady flame spread. A very sharp radiative flux distribution acts similarly to a pilot source, producing a steady state flame relatively quickly. In general, the mode of ignition has little, if any, effect on the final steady state flame spread assuming, of course, that the transition to flame spread occurs.

*This study is supported by the NASA Microgravity Science Program under the Inter-Agency Agreement No. C-32001-R. The technical monitor of this study is Ms. Sandra Olson at Lewis Research Center.*

## REFERENCES

1. Friedman, R., and Sacksteder, K. R., *Fire Behavior and Risk Analysis in Spacecraft*, NASA TM100944 (1988).
2. Kashiwagi, T., *Fire Safety J.* 3:185-200 (1981).
3. Kashiwagi, T., *Combust. Flame* 34:231-244 (1979).
4. Mutoh, N., Hirano, T., and Akita, K., *Seventeenth Symposium (International) on Combustion*, The Combustion Institute, Pittsburgh, 1978, pp. 1183-1190.
5. Akita, K., in *Aspects of Degradation and Stabilization of Polymers* (H. H. G. Jellinek, Ed.), Elsevier, 1978, Chap. 10.
6. de Ris, J. N., *Twelfth Symposium (International) on Combustion*, The Combustion Institute, Pittsburgh, 1969, pp. 241-252.
7. Bhattacharjee, S., and Altenkirch, R. A., *Twenty-Third Symposium (International) on Combustion*, The Combustion Institute, Pittsburgh, 1993, pp. 1627-1633.

8. Hamins, A., Fischer, S. J., and Kashiwagi, T., *Combust. Sci. Technol.* 97:37-62 (1994).
9. Nakabe, K., McGrattan, K. B., Kashiwagi, T., Baum, H. R., Yamashita, H., and Kushida, G., *Combust. Flame* 98:361-374 (1994).
10. Olson, S. L., Ferkul, P. V., and Tien, J. S., *Twenty-Second Symposium (International) on Combustion*, The Combustion Institute, Pittsburgh, 1988, pp. 1213-1222.
11. Kashiwagi, T., *Combust. Sci. Technol.* 8:225-236 (1974).
12. Wichman, I. S., and Baum, H. R., *Heat Transfer in Microgravity* (C. T. Avedisian and V. A. Arpaci, Eds.), HTD-269, ASME, New York, 1993, pp. 111-118.
13. Amos, B., and Fernandez-Pello, A. C., *Combust. Sci. Technol.* 62:331-343 (1988).
14. Shafizadeh, F., *J. Anal. Appl. Phys.* 3:283-305 (1982).
15. Kashiwagi, T., and Nambu, H., *Combust. Flame* 88:345-368 (1992).
16. Olson, S. L., *Combust. Sci. Technol.* 76:233-249 (1991).
17. Ferkul, P. V., and T'ien, J. S., *Combust. Sci. Technol.* 99:345-370 (1994).
18. Di Blasi, C., *Combust. Flame* 100:332-340 (1995).
19. de Ris, J. N., *Seventeenth Symposium (International) on Combustion*, The Combustion Institute, Pittsburgh, 1978, pp. 1003-1016.
20. Grayson, G. D., Sacksteder, K. R., Ferkul, P. V., and T'ien, J. S., *Microgravity Sci. Technol.*, VII 2:187-195 (1994).

Received 14 October 1994; revised 4 August 1995

